XI Interventional Radiology

Marilena Vendittelli

Sapienza Università di Roma

1 INTRODUCTION

Interventional Radiology (IR) refers to minimally invasive procedures performed under radiological image guidance. Surgical tools like needles, probes or catheters, are used to reach the target through the patient skin or through navigation inside anatomical structures like, e.g., blood vessels, under the guidance of ultrasound (US), computed tomography (CT), fluoroscopy (XA) or magnetic resonance (MR). IR procedures are today reliable alternatives to surgery for the diagnosis and minimally-invasive treatment of several neoplastic and non-neoplastic conditions in various organs, including liver, lung, kidney, pancreas, bone and breast.

Two broad classes of IR procedures are considered in these notes, according to the type of access: vascular and percutaneous. Among the most common vascular procedures restoring blood flow to the brain, kidneys and legs, it is worth citing angioplasty and stenting which consist in inserting a balloon catheter or a metal stent (or both) into the vessel under imaging guidance. Percutaneous interventions include diagnostic procedures, such as aspiration or core biopsy of tumors, and therapeutic procedures, such as collection drainage, embolization and tumor ablation through percutaneous probes that deliver lethal energy (through radiofrequency, cryoablation, microwave, laser, high-energy focused ultrasound and irreversible electroporation) to targeted lesions, causing tumor necrosis without damaging adjacent tissues or organs. The intra-operative imaging modalities are mainly US for soft tissue and superficial anatomic structures, otherwise XA, CT or MR are commonly used.

Indeed, despite the technical advances obtained in the field of diagnostic imaging in the last decades, operator experience and manual skills remain critical factors in the field of IR, with significant differences in terms of clinical success between differently experienced operators [Rizzo et al., 2011, McDonald et al., 2009, Rhim et al., 2004].

In addition, while US and XA offer real-time guidance but are somewhat limited in the visualization of deep organs and soft tissues, CT and MR are more effective in the visualization of normal anatomy and pathologies of visceral organs but do not support real-time image acquisition. This adds significant complexity to interventional procedures performed under CT and MR guidance, in particular in terms of accuracy of needle placement, and exposure to ionizing radiation.

The benefits related to the introduction of robotic technologies in this field range from increased accuracy in the tool placement, to protection of the staff from radiation, to procedure monitoring and optimization, and postoperative data analysis [Fichtinger et al., 2008]. Accuracy is increased by tracking manually operated tools or by using a robot for tool positioning and steering, while

teleoperation of the robotic system performing the procedure allows shielding the medical staff from radiations.

Due to the minimally invasive type of access and the imaging guide characterizing IR procedures, the specific challenges of IR robotic systems design involve:

- the robot kinematic architecture that must fit the workspace constrained by the imaging device and comply with the fixed point of access to the patient body;
- the configuration and positioning system with respect to the patient and the operating room setup;
- the sensors and actuators compatibility with the imaging modality;
- modeling and control methodologies for: tool motion planning and steering; compensation of physiological motions of organs and tissue deformation during tool placement; satisfaction of the fixed access point constraint while placing the tool;
- preoperative and intraoperative image fusion algorithms to allow intraoperative navigation;
- force sensing and rendering, in case of teleoperation;
- appropriate user interfaces providing haptic and visual feedback and possibly cues to the radiologist.

In the following sections, after providing a short overview of the existing robotic systems for endovascular (Sect. 2) and percutaneous procedures (Sect. 3) we will focus on the problem of needle-tissue interaction force reconstruction, one of the main challenges to fully exploiting robotics potentialities in percutaneous procedures (Sect. 4).

2 ROBOTIC SYSTEMS FOR ENDOVASCULAR PROCEDURES

Endovascular procedures are performed by inserting a flexible catheter inside anatomical structures, like blood vessels, to reach a target for diagnostic and/or therapeutic treatments mainly under XA guidance. Steerable catheters (see Tutorial 3) are used to deliver treatments in areas difficult to reach, like, e.g., inside the heart. Despite the progresses in catheters construction technology and in imaging systems performance, the accuracy and safety of the manual procedures are still highly dependent on the operator skills due to lack of real-time visual feedback. The need to protect the operator from radiations during the procedure prevents the use of continuous imaging acquisition.

Figure 1 – From left to right: Magellan, CorPath, Amigo, Niobe.

In recent years robotics systems have been developed to allow the physicians to remotely control the catheter while being shielded from unnecessary radiation exposure. Commercial systems include the **SENSEI** and **Magellan** robotic system by Hansen Medical (FDA cleared, acquired by Auris surgical in 2016). The Sensei is designed for interventional electrophysiology procedures, like e.g. the treatment of heart arrhythmia, while the Magellan is indicated for multi-specialty, peripheral vascular robotics procedures. The Artisan Extend Control Catheter and the Lynx ablation catheter work in conjunction with the SENSEI platform, are robotically steerable, and provide distal force sensing in electrophysiology procedures. The procedure is performed under XA guidance. The catheter is steered by controlling the tension of tendons routed through the two concentric sheaths guiding the catheter. The physician remotely controls the tip of the catheter using a 6D input device. The measured forces are visually rendered on the display and through vibratory feedback at the input device. Studies show that patients fluoroscopy time is also reduced. A similar system, the **CorPath**, FDA cleared and CE marked, has been developed by Corindus Vascular Robotics. The intended use is in coronary and peripheral vascular interventions.

The **Amigo** system is instead closer to traditional steering, making use of knobs for rotating, flecting/extending the catheter and buttons to advance it. If, on one side, this is more familiar and intuitive to physicians, on the other side it does not allow the possibility of a haptic feedback.

The **Niobe** system (Stereotaxis Inc.) for robot-assisted electrophysiology procedures uses remote magnetic catheter control. The system is composed of two robotically-controlled magnets close to the table. Uniform magnetic field is generated by arms motion for omnidirectional steering of a catheter magnetic tip inside the patient's body. XA provide imaging feedback on the catheter position.

Although the above systems have changed the standard of care in intravascular procedures, challenging aspects remain, like e.g., shape and force sensing on the whole catheter body, compensation of cardiac heart motion, transmission of sufficient force to execute the treatment.

3 ROBOTIC SYSTEMS FOR PERCUTANEOUS PROCEDURES

Conventional procedures are based on free-hand percutaneous placement of needles and probes under image guidance, either US, CT, XA or MR. Typically the operator identifies the target lesions in the planning phase, manually performs the procedure, possibly through multiple iterations, and assesses results and complications in a subjective manner. This approach exposes the whole procedure to significant risks of failure for several reasons, including inappropriate planning, patients' movements, operator fatigue and lack of quantitative data for procedure validation.

As in the case of vascular operations, the introduction of robots is beneficial for most of the drawbacks of manual procedures. It is worth noticing, however, that the design of kinematics, sensing and actuation systems for robots meant to support percutaneous procedures is more critical with respect to endovascular operations. The guiding mechanism must, in fact, work in close proximity to the

entry point and, hence, must fit the constrained space of the gantry. In addition, being the tools often rigid, or semirigid, they need to be reoriented while maintaining fixed the body entry point. This constraint is similar to the remote center of motion arising in minimally invasive surgery but without a trocar. The use of multimodal images, in addition, raises the problem of components compatibility. There exist today several systems for percutaneous interventions, either robotic or not, designed to work with MR, CT, XA, and US imaging devices. They can be grouped in two classes according to the positioning system: patient- and gantry- or floor-mounted systems. Systems inside each class differ for their compatibility with imaging devices, kinematic architecture, degree of autonomy, registration procedure, as discussed below.

3.1 Patient-mounted systems

These systems aim at reducing positioning errors due to tissue movement; the simplest devices are made of adhesive plates which can be attached to the patient's skin, around the entry point, featuring mechanisms which allows for needle guidance (either manual or automatic) and lock to the correct orientation. Given their positioning system, these devices are limited by weight and size.

Commercial devices are passive, and hence not robots. Examples include: **SimpliCT** commercialized by Neorad, for use with CT, PET-CT and Cone Beam CT, does not provide a physical but rather a laser guide to align the needle in the targeting direction; **Seestar,** by Apriomed, a device for CT guided biopsy based on the principle of rotating arches of half spheres that allow orbital needle positioning. For both these devices, the needle is oriented and inserted manually.

Research prototypes fill the class of active systems (see Fig. 2): the **Robopsy** system [Barret et al., 2005], for CT-guided percutaneous biopsies, is based on orbital needle positioning with two stepper motors for automated clamping and releasing of needle and its insertion, and allows the needle to move with organ motion after insertion. This system does not need registration to the scanner, but

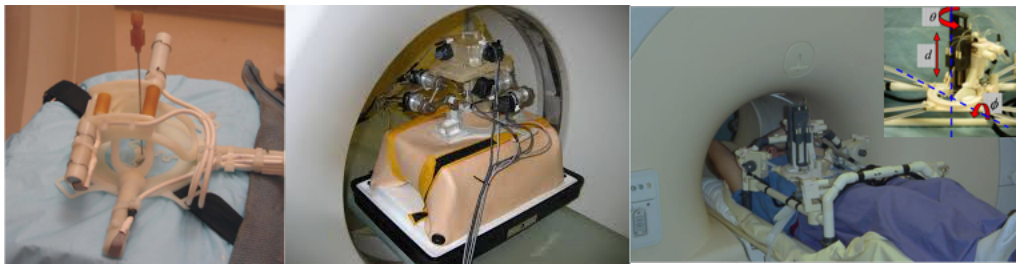

Fig. 2 – Patient-mounted research prototypes. From left to right: Robopsy, CT-Bot, LPR and close view of needle holder.

manual alignment is required for remote manual control of the needle, with feedback from CT images; the **CT-Bot** [Maurin et al., 2004], which comprises a CT-guided, 5-DOF parallel mechanism actuated by ultrasonic piezo motors with fiducial configuration for registration, plus a 2-DOF steering device for automatic insertion and spinning of the needle; the CT- and MR-compatible **Light Puncture Robot (LPR)** [Taillant 2004, Bricault 2008], with 4 drivers on a frame fixed to the

scanner table and a fiducial configuration for scanner registration. The last two systems are bulky and restrict the access to the gantry for operators, also encumbering part of the patient's bed.

3.2 Gantry- or floor-mounted systems.

Commercial systems (see Fig. 3). **INNOMOTION** [Melzer et al., 2008], for MR and CT guided interventions, was one of the first commercialized, CE cleared, fully MR compatible assistive device. The 6 DOFs are actuated by pneumatic motors. The robot arm is attached to a 260° arch that is mounted to the patient table of the scanner and can be passively prepositioned on either side of the arch according to the region of interest. Active positioning measurements are achieved via fiberoptic coupled limit switches, along with rotational and linear incremental sensors. The kinematics of the device has been developed for use in close bore MR scanners and the CT gantry. A front-end module for application of coaxial probes (e.g. cannulae for biopsies, RF or Laser Probe, endoscopes, etc.) provides two degrees of freedom and is attached to a robotic arm with 4 degrees of freedom. This architecture allows to keep the remote center of motion at the skin entry point. The insertion is manual. The system is no longer commercialized.

Fig. 3 – Gantry- or floor-mounted commercial systems. From left to right: INNOMOTION, SOTERIA, iSYS1, ROBIO.

The **SOTERIA** robot for MR-guided prostate biopsy, has four major features: MR-visible needle guide, MR-compatible robot, pneumatic valve system with PLC, and a control software allowing planning and automatic motion of the needle guide to the planned position. The robot is built as a hybrid system with serial and parallel kinematics (modified Stuart platform). Two pneumatic cylinders controllling the rotation and angulation of the needle guide holder are in a serial chain and are mounted over the tripod that is a parallel structure controlled by the other three motors. The tripod provides the translational movement of the needle guide. The motors are specifically designed for MR use and made of non-conductive plastic materials. The **iSYS1** for needle placement using CT or XA is characterized by a passive arm fixed to the CT bed with a 2 DOF front-end module automatically aligning the needle guide along the direction planned by the accompanying software. The position device can also be remotely operated by the medical staff. The insertion is manual. The Perfint **RobioEX** and **Maxio** (FDA approved) are floor-mounted 5-DOF assisting devices for CT and PET-CT guided needle positioning including image-based registration and planning software.

Research prototypes (see Fig. 4). The prototype system developed by **Siemens** [Loser and Navab, 2000] for XA guided biopses features a pivoting parallelogram with a 2-DOF remote center of motion and a needle guide. It can be controlled via

joystick or automatically using visual servoing, an image-based control approach, and therefore does not require registration. The robotics laboratory of ARC Seibersdorf Research in Austria developed the **B-Rob** series, for needle placement using CT or US. The technology was later licensed by iSYS Medizintechnik GmbH and redesigned in the commercial systems iSYS and iSYS1 previously cited.

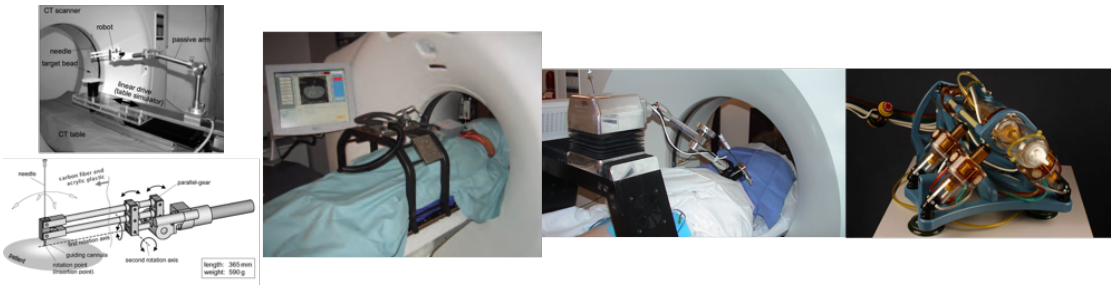

Fig. 4 - Gantry- or floor-mounted prototypes. From left to right: Siemens prototype with the front-end module kinematic design, B-Rob, AcuBot, MrBot.

AcuBot [Stoianovici et al., 2007], for active needle insertion under CT or XA, is a 5-DOF robotic needle-placement system operating by a bridge frame over the patient bed. The procedure is based on aligning the needle held by the robot with the laser markers of the CT scanner. The robot can then automatically orient the needle toward a target selected in a CT slice. The 6-DOF **MrBot**, has been developed at JHU for fully-automated, MR-guided, transperineal prostate percutaneous access [Stoianovici et al., 2007]. For MR compatibility the robot is exclusively constructed of nonmagnetic and dielectric materials such as plastics, ceramics, and rubbers and is electricity free. The system utilizes a new type of pneumatic step motors (PneuStep). Fiber optic encoding is used for feedback, so that all electric components are distally located outside the imager's room. Recently the FDA has approved the MrBot for the biopsy trial successfully performed in 5 patients.

4 TOWARD TELEOPERATED NEEDLE INSERTION

As discussed in the previous sections, existing systems are still limited under many aspects. Ideally, a robotic platform for interventional procedures should feature real-time or near real-time guidance and visualization of the operatory field, force feedback, compliance with patient motion and compensation of target displacement, inter-modality compatibility and indication to various types of procedures in several anatomical regions.

Teleoperated needle insertion can comply with the above requirements as it allows to operate under real-time image guidance (e.g., XA), while protecting the medical staff from radiations. In addition, an appropriate kinematic design and control of the slave robot can fit the very constrained environment of an MR gantry without constraining the operator mobility.

With a remote insertion, however, the operator would lose any kind of haptic feedback. The teleoperated procedure performance can considerably benefit from the combination of imaging and needle-tissue interaction force information

[Gerovich et al., 2004]. The introduction of force sensors however increases cost and size of the robotic system. Moreover, classical F/T sensors placed at the base of the needle cannot provide the information of the force exchanged at the tip, due to the friction along the needle shaft. Understanding the insertion mechanics and estimating the needle-tissue interaction forces is one fundamental challenge in the development of systems for needle insertion assisted by robots, either remotely operated or autonomously performing the procedure. In the followig, after a short review of needle-tissue interaction modeling of Sect. 4.1 and Sect. 4.2, online model identification methods for interaction force prediction and feedback enhancement are introduced in Sect. 4.3.

4.1 Mechanics of needle-tissue interaction

The study of needle-tissue interaction phenomenon has generated a quite wide literature both focused on experimental observation and on the challenging task of capturing the most relevant effects in an analytical model. Part of the essential contributions are reported in Sect. 4.2.

The experimental observation, as demonstrated in [Gerwen, 2013], is not an easy task both for the difficulties of obtaining significant data (particularly on living human tissues) and because the experimental conditions are extremely difficult to control for a clear interpretation of the collected data. The same reference proposes an interesting point of view on the experimental aspects of needle-tissue interaction, together with a quite exhaustive literature review.

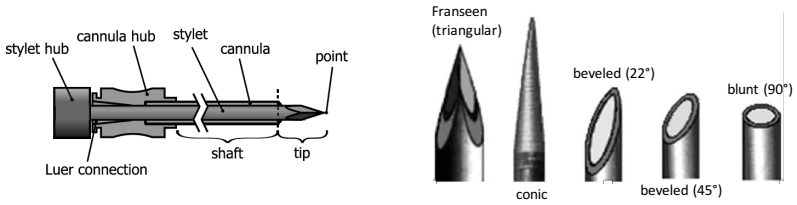

Fig. 5 - Main parts of a needle (left), and different tip shapes (right) [Gerwen, 2013].

In this section, we will briefly recall the interaction mechanics of hollow needles with soft tissues while providing a synthetic overview of the modeling effort done by researchers. Figure 5 (left) shows the main parts of a typical needle used in interventional radiology procedures and the most common tip shapes (right). The stylet is optional: the needle can be either a trocar (outer beveled or nonbeveled cannula and a three-sided stylet tip shape, as in Fig. 5) or a single-wall type (with beveled tip).

The main phases of a needle insertion procedure are shown in Fig. 6. The insertion starts upon contact of the needle tip with the tissue boundary. During the contact phase the boundary deflects under the action of the needle which is not yet penetrating the tissue. The interaction force and the tissue stress increase with the needle displacement. This phase ends when the boundary is breached (puncture event) due to the tissue stress exceeding a characteristic threshold. A crack then starts in the tissue and the needle penetrates with a sudden drop in the

interaction force. The post-pucture crack growth depends on the local tissue properties and on the energy stored in the pre-puncture phase. During tip and shaft insertion the needle tip is subject to cutting forces while a friction force arises due to the increasing contact area between shaft and tissue. A friction force of the same nature, with opposite sign, acts on the needle shaft during the extraction phase. Figure 6 (right) shows a typical evolution of the total force along

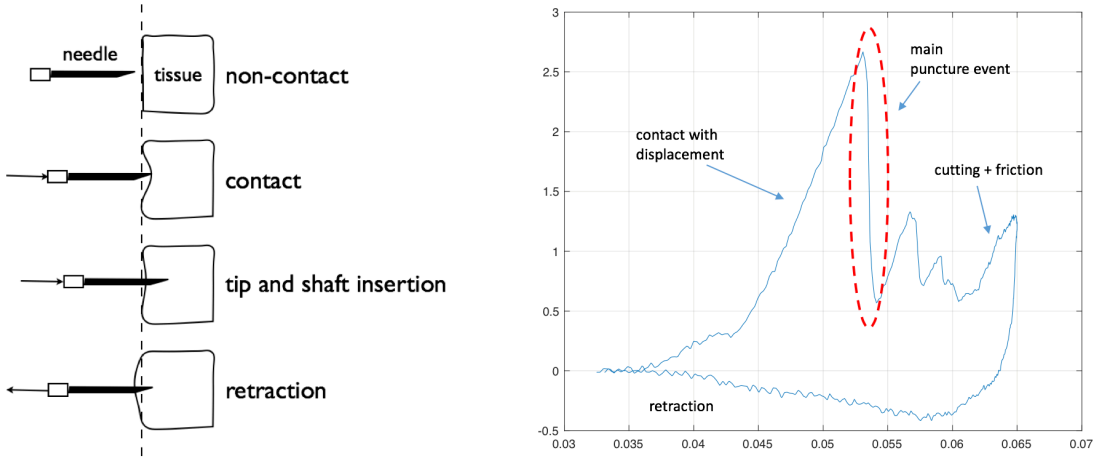

Fig. 6 - Phases of a needle insertion procedure (left) and a typical force-displacement curve (right).

the needle shaft plotted against the displacement. The information is provided by a force sensor placed at the base of the needle. A quite complete dynamic model of the insertion mechanics is provided in [Khadem et al., 2016].

A large number of variables affect the mechanics of the insertion including tissue characteristics (artificial vs biologic, human vs animal, dead vs living, etc.), needle type, insertion method, insertion velocity, needle axial rotation, insertion location and direction, bevel orientation. A comprehensive review is offered in [Gerwen, 2013]. Later in these notes we will recall with some detail the analytic description of the rupture force dependence on the insertion velocity presented in [Mahvash and Dupont, 2010] and [Khadem et al., 2016].

A consistent work has also been devoted to the determination of load distribution along the needle and the nature of the insertion force components. Using finite elements models and measurements of tissue displacements various authors, including [DiMaio and Salcudean, 2003] and [Crouch et al., 2005], reported a largely uniform distribution along the shapft, with the exception of the tip where a higher load is observed, likely due to cutting.

The uniform distribution along the shaft has been related to friction. Although neglected in some studies [Misra et al. 2010; Moore at al., 2011; Heverly et al., 2005], this component of the insertion force is however useful, among others, to verify that the axial laod, proved to be uniform for artificial tissues, can also be considered as such in case of biological tissues. A uniform load distribution would, in fact, result in a linear increase of friction with the contact area. Using different methods it has been shown that the total insertion force is composed of a constant

(at steady state) force due to cutting and a linearly increasing force due to friction [Hing at al., 2006; Kobayashi et al., 2009; Okamura et al., 2004; Abolhassani et al., 2007], and that this composition of the force can be assumed also for biological tissues.

Although the experimental findings and validation seem to agree on the qualitative evolution of the forces exchanged during the insertion of a hollow needle, the modeling effort may differ in the methodology used for their derivation, in the intended use of models and in the assumptions taken. Although all the developed models have their merits and limits and, depending on the intended use, one model might be preferable to another, in the following section we will report on the analytical description of the needle-tissue interaction phases for their high level of abstraction and their computational efficiency suiting the need of real-time force rendering in a teleoperated architecture.

4.2 Analytical models

With reference to Fig. 7 and starting from the contact phase, the interaction forces exchanged at the needle tip and along the shaft during the insertion are: the puncturing force F_p exchanged at the endpoint of the needle tip during the contact phase when the tissue boundary is displaced by the needle tip; the cutting force F_c at the tip including crack propagation into the tissue in response to needle displacement; the friction force F_f tangent to the needle shaft; the tissue deformation force F_s applied perpendicularly to the contact surface between the needle shaft and the tissue.

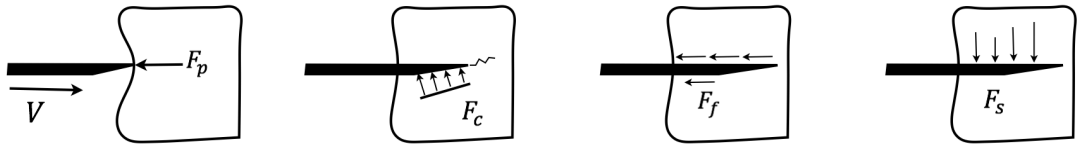

Fig. 7 - Interaction forces during needle insertion

The contact, or puncturing force F_p is commonly represented by the visco-elastic models reported in Table 1. The position of the tip is denoted by $p(t)$, the parameters $k, b, \alpha, \beta, \gamma, n$, are constant characterizing the tissue properties.

Table 1 - Visco-elastic models of contact.

Model	Equation
Elastic	$F_p = k\,p(t)$
Kelvin Voigt	$F_p = k\,p(t) + b\dot{p}(t)$
Kelvin Boltzman	$F_p = \alpha\,p(t) + \beta\dot{p}(t) - \gamma\dot{F}_p$
Maxwell	$F_p = k\,p(t) + \alpha\dot{F}_p$

Hunt-Crossley	$F_p = k\,p^n(t) + \lambda p^n(t)\dot{p}(t)$

The cutting force F_c includes the crack advancing phenomenon. In [Khadem et al., 2016] a criterion based on the rate of energy release per unit length of crack advance has been used to estimate the cutting force applied to the needle tip. Assuming the insertion velocity is appropriately high, the tissue near the needle tip is modeled as a linear elastic material and, for insertion depth higher enough than the depth at which the crack initiate, the cutting force is the constant $F_c = \frac{4\,\tan\alpha/2 E_R^2}{E_T}$, where E_T is the tissue stiffness per unit length and α the needle bevel angle. The complete, time-dependent expression of F_c is provided in [Khadem et al., 2016].

The friction forceF_f, is usually described through the LuGre model

$$\dot{z} = V - \sigma_0 \frac{|V|}{g(V)} z \qquad F_f = \sigma_0 z + \sigma_1 \dot{z} + \sigma_2 V$$

where V can be considered as the needle insertion velocity, z is the internal friction state, σ_0 the stiffness associated to the microscopic tissue deformations and σ_1 the micro damping, and σ_2 is the viscous damping coefficient. The function $g(V)$ captures Coulomb friction and Stribeck effect: $g(V) = f_c + (f_s - f_c)e^{-\Upsilon|V|}$ where f_s and f_c are respectively the stiction and Coulomb friction, and Υ is a constant related to the convergence velocity of $g(V)$ to f_c.

Models of transverse force F_s are mainly used to predict the deflection of flexible needles and in [Kahdem et al. 2016] it is modeled as the sum of the constant needle-tissue interaction force per unit length of the needle and a term proportional to the time derivative of bending.

When considering multi-layered tissues, an effective model easy to implement and numerically efficient and especially suited for simulations is provided in [Gerovich et al., 2004] and synthetically described in Fig. 8.

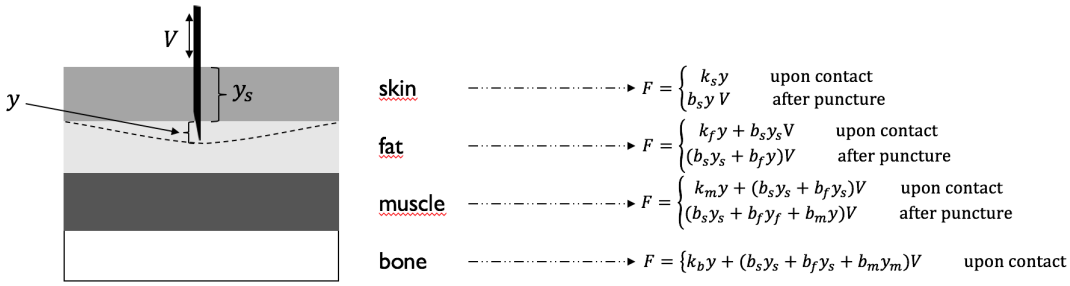

Fig. 8 – A multi-layer needle-tissue interaction model: y is the needle tip penetration, y_i the length of the shaft inside each layer, k_i and b_i the viscoelastic parameters of each layer, $i = \{s, f, m, b\}$ the tissue layer index.

4.3 Online needle-tissue interaction model identification

The models given in the previous section rely on the knowledge of physical parameters characterizing the tissue. These parameters are not always available in advance or known with the needed accuracy. This section summarize an online

identification method [Barbé et al., 2007] used to predict the interaction force in unknown tissues and to detect layer transitions. The detection of a rupture event is useful when puncturing is the surgical task like, e.g., in an epidural puncturing , while the prediction of a puncturing is useful to prevent perforation of critical structures like, e.g., vessels inside an organ where the needle is being inserted. In addition, in multylayered tissues the detection of a transition allows to remove the force generated by the shaft motion in contact with the already penetrated layers so as to obtain a force reconstruction at the tip [Cacciotti et al., 2018], the most relevant information when inserting a needle.

Assuming a perfectly rigid needle, it is possible to consider only forces directed along the needle shaft. Two major forces are considered in the identification model: the puncturing force F_p described in the previous section and modeled as an elastic force, and a damping force including viscous friction along the needle shaft and cutting forces. Let $p(t)$ be the position of the needle tip over time and p_0 the position of the needle tip when in contact with the first layer. The interaction force F is described by a generalized Kelvin-Voigt (KV) model with variable stiffness and damping coefficients and can written as $F = \varphi(t)^T\theta(t)$, with $\varphi(t) = (-p(t) \quad -\dot{p}(t))^T$ the vector of needle tip position and velocity and $\theta(t) = (k(t) \quad b(t))^T$ the vector of parameters to be identified. Force prediction is obtained using a standard Recursive Least Square (RLS) algorithm.

At step $i > 0$, the estimation of parameters vector $\hat{\theta}_i$ and the definite-positive covariance matrix Ψ_i can be computed as

$$\hat{\theta}_i = \begin{pmatrix} \hat{k}_i \\ \hat{b}_i \end{pmatrix} = \hat{\theta}_{i-1} + \frac{\Psi_{i-1}\varphi_i e_i}{\lambda_i + \varphi_i^T \Psi_{i-1}\varphi_i} \qquad \Psi_i = \Psi_{i-1} + \frac{\Psi_{i-1}\varphi_i\varphi_i^T\Psi_{i-1}}{\lambda_i + \varphi_i^T\Psi_{i-1}\varphi_i}$$

where $\lambda \in (0,1]$ is a forgetting factor. The error is defined as $e_i = F_i - \hat{F}_i$, where $\hat{F}_i = \varphi_i^T\hat{\theta}_{i-1}$ is the prediction of the interaction force. To allow the estimation of the time-varying model parameters it is necessary to include in the basic RLS algorithm a covariance resetting mechanism, while the introduction of a dead-zone for the covariance matrix estimation is introduced to keep the estimation algorithm robust with respect to noise (see [Barbé et ., 2007] and the reference therein).

The force predicted using the RLS identification algorithm and the estimation error can be used to detect abrupt changes in the interaction force which, as described in the previous section, correspond to a puncture event. A first event occurs at the surface of the tissue but multiple events may occur also after the penetration of the needle in case of a multi-layered tissue, indicating a transition from one layer to the next.

The analysis of the statistical characteristics of the prediction error e_i leads to the detection of layer transitions. Considering the error as a residual signal belonging to a normal distribution and defined a "distance" function $s_i = e_i^2$, a transition is detected when

$$\gamma < g_i = \begin{cases} 0, & \text{if } i = 0 \\ \max(g_{i-1} + s_i - \nu, 0) & \text{otherwise} \end{cases}$$

In the above equation, $\gamma = \frac{\sigma_1^2 - \sigma_0^2}{2}$ and $\nu = \frac{\sigma_1^2 + \sigma_0^2}{2}$ with σ_1 and σ_0 respectively the error variance with and without the occurrence of a rupture event. Hence, the accuracy of the detection depends on the knowledge of the error distribution parameters. Figure 9 shows the result of the detection algorithm during needle insertion in bovine muscle tissue.

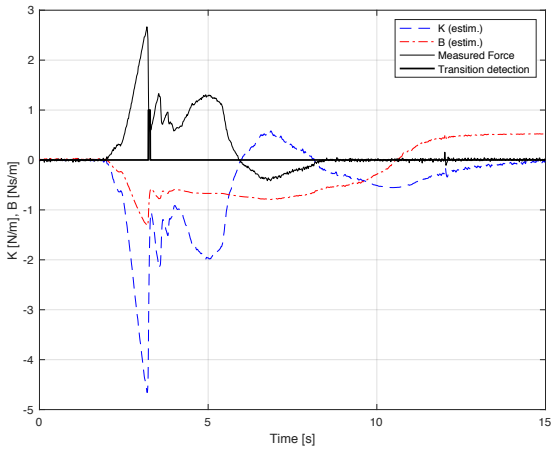

Fig. 9 - Detection of a puncturing event (black), and time evolution of the model parameters.

The above described detection algorithm has been used in [Barbé et ., 2007] to augment the teleoperation scheme by amplifying the force rendered to the master upon the detection of a rupture event. At the same time the reference position of the slave is kept constant to avoid excessive penetration of the needle at the rupture. In the same line, an enhancement of the force feedback can be obtained by subtracting the reconstructed friction force to improve the perception of the elastic component of the force indicating contact with a new layer, thus mimicking the function of a coaxial needle [Cacciotti et al., 2018].

5 Bibliography

Abolhassani N., Patel R., and Moallem M. (2007). Needle insertion into soft tissue: A survey. *Med Eng Phys*, 29, 413–431.

Barbé L., Bayle B., de Mathelin M. Gangi A. (2007). *In Vivo* Model Estimation and Haptic Characterization of Needle Insertions. *The International Journal of Robotics Research*, 26, 1283–1301.

Barrett S.R.H., Hanumara N.C., Walsh C.J., et al. (2005). A remote needle guidance system for percutaneous biopsies. *ASME (IDETC/CIE)*.

Bricault I., et al. (2008). A light puncture robot for CT and MRI interventions. *IEEE EMBM*, 27(3), 42–50.

Cacciotti N., Cifonelli A., Gaz C., Paduano V., Russo A.V., Venditelli M. (2018). Enhancing force feedback in teleoperated needle insertion through on-line identification of the needle-tissue interaction parameters. *7th IEEE RAS/EMBS Int.*

Conference on Biomedical Robotics and Biomechatronics (BIOROB 2018).

CROUCH J. R., SCHNEIDER C. M., WAINER J., OKAMURA A. M. (2005) A velocity-dependent model for needle insertion in soft tissue. *Med Image Comput Comput Assist Interv*, 8, 624-32.

DIMAIO S. P., SALCUDEAN S. E. (2003). Needle insertion modeling and simulation. *IEEE Trans Robotic Autom*, 19(5), 864–875.

FICHTINGER G., KAZANZIDES P., OKAMURA A., HAGER G., WHITCOMB L., TAYLOR R. (2008). Surgical and interventional Robotics: Part II, *IEEE Robotics & Automation Magazine*, 15(3), 94-102.

GEROVICH O., MARAYONG P., OKAMURA A. M. (2004). The effect of visual and haptic feedback on computer-assisted needle insertion. *Computer Assisted Surgery*, 9(6), 243-249.

HEVERLY M., DUPONT P., TRIEDMAN J. (2005). Trajectory optimization for dynamic needle insertion, *IEEE International Conference on Robotics and Automation*.

HING J. T., BROOKS A. D., DESAI J. P. (2006) Reality-based needle insertion simulation for haptic feedback in prostate brachytherapy. *IEEE International Conference on Robotics and Automation*.

KHADEM M., ROSSA C., SLOBODA R., USMANI N., TAVAKOLI M. (2016). Mechanics of Tissue Cutting During Needle Insertion in Biological Tissue, *IEEE Robotics and Automation Letters,* 1(2), 800-807.

KOBAYASHI Y., SATO T., FUJIE M. G. (2009). Modeling of friction force based on relative velocity between liver tissue and needle for needle insertion simulation. *31st Annual International Conference of the IEEE EMBS*.

LOSER M.H., NAVAB N. (1991) A new robotic system for visually controlled percutaneous interventions under CT fluoroscopy. *MICCAI*.

MAGNUSSON A., et al. (1991). CT-guided core biopsy using a new guidance device. *Acta Radiol*., 32(1), 83–85.

MAHVASH M. AND DUPONT P. (2010) "Mechanics of dynamic needle insertion into biological material," *IEEE Transactions on Biomedical Engineering*, 57(4), 934–943.

MAURIN B., PICCIN O., BAYLE B., et al. (2004).A parallel 5-DOF positioner for semi spherical workspaces. *ASME (IDETC/CIE)*.

MCDONALD R.J., GRAY L.A., CLOFT H.J., THIELEN K.R., KALLMES D.F. (2009). The effect of operator variability and experience in vertebroplasty outcomes. *Radiology*, 253(2), 478-485.

MELZER A, et al. (2008). INNOMOTION for percutaneous image-guided interventions – principles and evaluation of this MRand CT-compatible robotic system. *IEEE Eng Med Biol*, 27(3), 66–73

MISRA S., REED K., SCHAFER B., RAMESH K., OKAMURA A. (2010). Mechanics of flexible needles robotically steered through soft tissue. *Int. J. Rob. Res*., 29(13), 1640–1660.

MOORE J. Z., MALUKHIN K., SHIH A. J., EHMANN K. F. (2011) Hollow needle tissue insertion force model, *(CIRP) Annals – Manufacturing Technology*, 60(1) 157 –160.

OKAMURA A. M., SIMONE C., O'LEARY M. D. (2004). Force modeling for needle insertion into soft tissue. *IEEE Trans Biomed Eng* , 51(10),1707–1716.

RHIM H, DODD GD 3RD, CHINTAPALLI KN, WOOD BJ, DUPUY DE, HVIZDA JL, SEWELL PE, GOLDBERG S.N. (2004). Radiofrequency thermal ablation of abdominal tumors: lessons learned from complications. *Radiographics*, 24(1), 41-45.

RIZZO S., PREDA L., RAIMONDI S., MERONI S., BELMONTE M., MONFARDINI L., VERONESI G., BELLOMI M. (2011). Risk factors for complications of CT-guided lung biopsies. *Radiol Med*., 116(4), 548-563.

STOIANOVICI D, et al. (2007). "MRI Stealth" robot for prostate interventions. *Minim Invasive Ther Allied Technol.,*16, 241-8.

TAILLANT E., et al. (2004). CT and MR compatible light puncture robot: architectural design and first experiments. *International Conference on Medical Image Computing and Computer-Assisted Intervention (MICCAI).*

van GERWEN D.J. (2013). Needle-Tissue Interaction by Experiment, Ph.D. Thesis, https://doi.org/10.4233/uuid:c2dac8ee-0529-49ae-8374-2d49efd0ba90.